Spin-Crossover and Field-Induced Single-Molecule Magnet Behaviour in Metal(II)-Dipyrazolylpyridine Complexes

Haiet Douib, Louis Cornet, Jessica Flores Gonzalez, Elzbieta Trzop, Vincent Dorcet, Abdelkrim Gouasmia, Lahcène Ouahab, Olivier Cador, Fabrice Pointillart

10.1002/ejic.201800819

FULL PAPER

Spin Crossover and Field-Induced Single-Molecule Magnet Behaviour in Metal(II)-Dipyrazolylpyridine Complexes

Haiet Douib,[a,b] Louis Cornet,[a] Jessica Flores Gonzalez,[a] Elzbieta Trzop,[c] Vincent Dorcet,[a] Abdelkrim Gouasmia,[b] Lahcène Ouahab,[a] Olivier Cador,*[a] Fabrice Pointillart,*[a]

Abstract: The reaction between the 2,6-di(pyrazol-1-yl)-4-(bromomethyl)pyridine (**L**) ligand and divalent transition metal salts led to the formation of three mononuclear complexes of formula $[M(\mathbf{L})_2](BF_4)_2{\cdot}xMeNO_2$ (M = Fe^{II} (**1·xMeNO₂**), x = 0 and 4, M = Co^{II}, x = 2 (**2·2MeNO₂**) and). Static magnetic measurements highlighted thermal spin crossover at high temperature (320-340 K) for the two Fe^{II} solvatomorphs nevertheless both the solvation degree and crystal packing had drastic influence on the shape and width of the hysteresis loop. Thus the **1** displayed abrupt and straight (6 K) hysteresis loop while for **1·4MeNO₂** the thermal spin transition could be described as a six-step gradual transition with the widest magnetic bistability range (35 K) for this kind of complexes. Irradiation at 530 nm of **1·4MeNO₂** provoked an efficient LIESST effect at low temperature (T_{LIESST} = 55 K). Finally dynamic magnetic measurements of **2·2MeNO₂** shown a field-induced mononuclear Single-Molecule Magnet behavior with Δ = 14.6(4) cm^{-1} and $\tau_0 = 6.28(8) \times 10^{-7}$ s.

Introduction

Molecular magnetic bistability is intensively studied by both chemist and physicist communities of the molecular magnetism due to the wide potential applications such as high-density memory capacities.[1] Such magnetic behaviour could be observed under different stimuli. Thus under magnetic field, Single-Molecule Magnets (SMMs)[2] is targeted while Spin CrossOver (SCO)[3] is the intended behaviour under temperature variation or light irradiation among other stimuli (pressure…).

The SCO behaviour is a well-known phenomenon since the 1930s.[4] By restricting the external stimuli to the temperature and light irradiation, the magnetic bistability can be thermodynamically (thermal SCO) and kinetically (photo-induced SCO called light-induced excited spin state trapping, LIESST)[5] reached. The magnetic bistability is driven mainly by the cooperativity induced by intermolecular interactions in the crystal lattice. All the metallic ion with the d^4-d^7 electronic configuration are potential candidates to SCO behaviour nevertheless the most popular metal ion is unambiguously the Fe^{II} because it allows the largest variation of the spin value involving paramagnetic and diamagnetic states (S = 2 → S = 0). Obviously, the choice of the nature of the ligand is crucial to impose an adequate crystal ligand field to the Fe^{II}. Thus the bpp-R ligand (where the bpp-R is a 2,6-di(pyrazol-1-yl)pyridine derivative is one of the most used ligand to be associated with the Fe^{II} ion leading to $[Fe(bpp\text{-}R)_2]^{2+}$ series of complexes.[6] The reason of the high popularity of such series of complexes is due to its ability to show thermal (near room temperature) and photo-induced spin crossover as well as the chemical-dependence of the spin transition. Therefore the observation or not of the spin transition and the temperature at which the spin transition could occur strongly depend of the substituent of the bpp moiety,[7] the nature of the solvent of the crystal lattice,[8] the nature of the anions[9] and the Jahn-Teller distortion[10].

Since the discovery of magnetic bistability at low temperature for a mononuclear lanthanide complex,[11] the interest for such simple systems were growing rapidly. Thus chemist community started to study mononuclear complexes of 3d ions to design SMMs. These systems mainly involved high-spin Mn^{III},[12] Fe^{III},[13] Fe^{II},[14] Fe^{I},[15] Ni^{I},[16] Ni^{II},[17] Co^{I} [18] and Co^{II}[19] ions. The last Co^{II}-based SMMs highlighted a large number of coordination for the metal ion ranging from two to eight[20] nevertheless the slow magnetic relaxation is usually observed under applied DC field to cancel the quantum tunnelling relaxation except for few examples of organometallic complexes[21]. Slow magnetic relaxation of the magnetization was rarely observed in system combining one 2,6-di(pyrazol-1-yl)pyridine derivative (bpp-R) and Co^{II}[22] and the probe of magnetic properties for $[Co(bpp\text{-}R)_2]^{2+}$ complexes is very scarce in literature[23].

The aim of our final project is to combine both SMM and SCO behaviour in a unique system by functionalizing the 2-(4,5-(4,5-bis(propylthio)-tetrathiafulvalenyl)-1H-benzimidazol-2-yl)-pyridine molecular skeleton by alkylation of the amine with a bromo-methyl-derivative such as the 2,6-di(pyrazol-1-yl)-4-(bromomethyl)pyridine (**L**).[24] A new approach is now to prepare the metal complexes involving the **L** ligand which could be therefore used as precursors to perform metallo-alkylation of our molecular skeleton. In the following lines, we reported the X-ray structures and the (photo)magnetic properties of two of such potential metallo-precursors of formula $[M(\mathbf{L})_2](BF_4)_2{\cdot}xMeNO_2$ (M = Co^{II}, x = 2 and M = Fe(II), x = 0 and 4).

[a] H.D., L.C., J.F.G., V.D., L.O., O.C. F.P.
Univ Rennes, CNRS, ISCR (Institut des Sciences Chimiques de Rennes) - UMR 6226, F-35000 Rennes, France.
fabrice.pointillart@univ-rennes1.fr
[b] H.D., A.G.
Laboratoire des Matériaux Organiques et Hétérochimie (LMOH), Département de sciences de la matière, Université de Tébessa, Rue de Constantine 12002, Tébessa, Algérie.
[c] E.T.
Institut de Physique de Rennes, Université de Rennes 1, UMR UR1-CNRS 6251, Rennes, France.

Supporting information for this article is given via a link at the end of the document.

Results and Discussion

Crystal structure

Slow diffusion of Et_2O vapor into $MeNO_2$ solution of $[Fe(\mathbf{L})_2](BF_4)_2$ yields mixtures of brown plate $[Fe(\mathbf{L})_2](BF_4)_2$ and prism $[Fe(\mathbf{L})_2](BF_4)_2{\cdot}4MeNO_2$ single crystals with variable ratio.

$[Fe(L)_2](BF_4)_2$ (1). Compound **1** crystallizes in the orthorhombic space group Pbcn (N°60) (Table 1). The ORTEP drawing of **1** is shown in Figure 1a. The asymmetric unit is composed of one half molecule of $[Fe(\mathbf{L})_2]^{2+}$ and one BF_4^- anion.

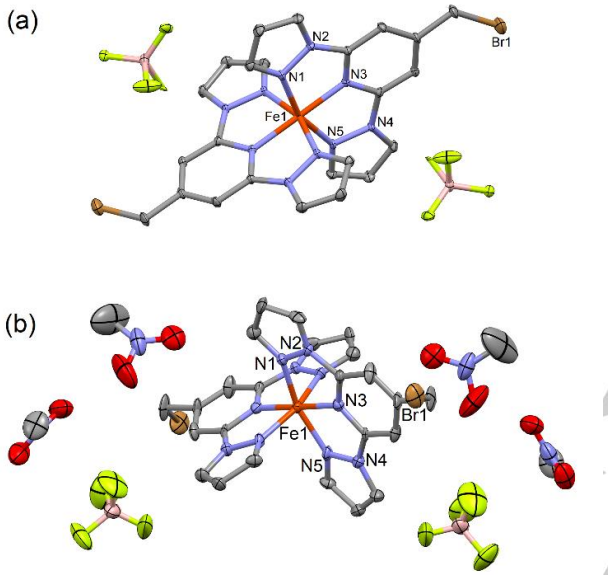

Figure 1. Ortep View of the structures of **Fe** (a) and **Fe·4MeNO₂** (b). Atomic displacement ellipsoids are drawn at the 30% probability level. Hydrogen atoms are omitted for clarity.

The Fe^{II} centre is coordinated to two trischelating ligands conferring a N6 surrounding. The average Fe-N bond lengths is equal to 1.947(3) Å with a slight difference between the Fe-$N_{(py)}$ distances (1.888(3) Å) which are shorter than the Fe-$N_{(pz)}$ distances (1.969(3) Å) due to the difference of Lewis basis strength between a pyridine and a pyrazole unit. Such bond lengths strongly suggest that the Fe^{II} ion is in its low-spin state (S = 0) at 200 K in the Fe compound. The characteristic $N_{(pz)}$-Fe-$N_{(pz)}$ and $N_{(py)}$-Fe-$N_{(py)}$ angles have been measured to 160.3(1)° and 174.6(1)° respectively. The two coordinated **L** ligands are perpendicular. The CH_2Br substituent is localized in the plan formed by the bpp fragment (Figure 2b).

The crystal packing of **1** highlights the formation of stack of molecules into a pseudo "terpyridine embrace" lattice *i.e.* a packing which is dominated by face-to-face π-π interactions and edge-to-face C-H···π contacts between the pyrazole moieties of neighbouring complexes.[25] The regular "terpyridine embrace" lattice form a stacked layers of molecules[26] while for the **1** compound the π-π stacking takes only place along one direction (Figure 2a). Interestingly, in a perpendicular direction (along the *a* axis) to the pseudo "terpyridine embrace" lattice, Br···Br short contacts (3.617 Å) are identified and could have consequences in the magnetic behavior.[7]

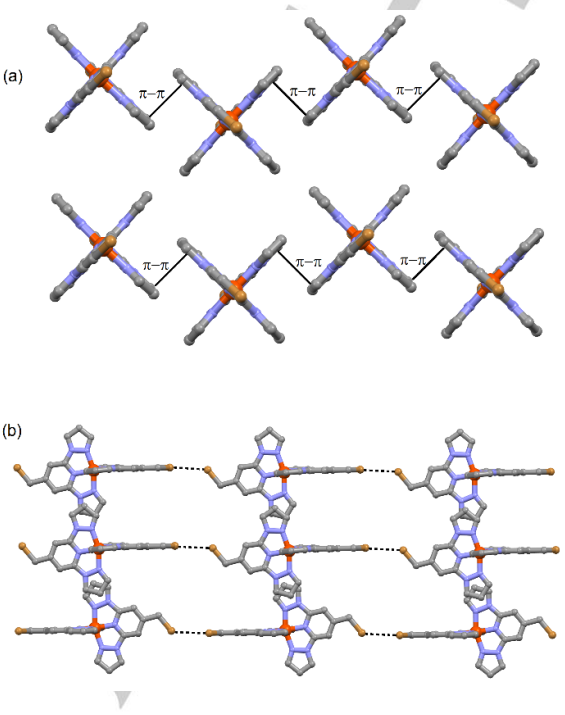

Figure 2. Crystal packing of **1** highlighting the pseudo "terpyridine embrace" (a) and the Br···Br short contacts (b).

Table 1. X-ray crystallographic data for the complexes **1, 1·4MeNO₂** and **2·2MeNO₂**.

Compounds	$[Fe(\mathbf{L})_2](BF_4)_2$ **(1)**	$[Fe(\mathbf{L})_2](BF_4)_2{\cdot}4MeNO_2$ **(1·4MeNO₂)**	$[Co(\mathbf{L})_2](BF_4)_2{\cdot}2MeNO_2$ **(2·2MeNO₂)**
Formula M / g.mol^{-1}	$C_{24}H_{20}F_8FeN_{10}Br_2B_2$ 837.77	$C_{28}H_{32}F_8FeN_{14}O_8Br_2B_2$ 1081.96	$C_{26}H_{26}F_8CoN_{12}O_4Br_2B_2$ 962.96
Crystal system	Orthorhombic	Orthorhombic	Triclinic
Space group	Pbcn (N°60)	Iba2 (N°45)	P-1 (N°2)
Cell parameters	a = 18.0328(3) Å b = 10.2933(2) Å c = 15.7133(3) Å	a = 15.3072(18) Å b = 16.2477(19) Å c = 16.3779(17) Å	a = 8.0294(6) Å b = 8.8561(7) Å c = 25.623(2) Å α = 90.508(3) β = 96.528(2) γ = 97.459(2)
Volume/Å^3	2916.7(9)	4073.3(8)	1794.4(2)
Z	4	4	2
T / K	200 (2)	150(2)	150(2)
2θ range/°	6.54 ≤ 2θ ≤ 53.99	4.99 ≤ 2θ ≤ 58.68	4.64 ≤ 2θ ≤ 55.01
ρ_{calc} /g.cm^{-3}	1.908	1.764	1.782
μ / mm^{-1}	3.346	2.435	2.799
Number of reflections	47488	40076	39301
Independent reflections	3175	4618	8250
R_{int}	0.0282	0.0639	0.0584
$Fo^2 > 2\sigma(Fo)^2$	2839	4395	6763
Number of variables	250	286	496
R_1, wR_2	0.0572, 0.1898	0.0350, 0.0879	0.0450, 0.0934

$[Fe(L)_2](BF_4)_2{\cdot}4MeNO_2$ (1·4MeNO₂). **1·4MeNO2** crystallizes in the orthorhombic space group Iba2 (N°45) (Table 1). The ORTEP drawing of **1·4MeNO₂** is shown in Figure 1b. The asymmetric unit

10.1002/ejic.201800819

is composed of one half molecule of $[Fe(\mathbf{L})_2]^{2+}$, one BF_4^- anion and two nitromethane molecules of crystallization. Both solvated **1·4MeNO₂** and unsolvated **1** complexes are very similar. No significant difference of Fe-N distances are identified between the two complexes (Fe-$N_{(py)}$ = 1.895(3) Å and Fe-$N_{(pz)}$ = 1.942(3) Å) and thus the Fe^{II} centre is in its LS state at the temperature of the X-ray structure resolution (150 K). The characteristic $N_{(pz)}$-Fe-$N_{(pz)}$ and $N_{(py)}$-Fe-$N_{(py)}$ angles have been measured to 161.3(1)° and 179.6(1)° respectively. The two coordinated **L** ligands formed an angle of 79.2(4)°. Significant local structural changes are identified compared to **1** which should induce significance variation in the crystal filed around the Fe^{II} ion. The CH_2Br substituent is localised at 58.7° of the plan formed by the bpp fragment which is one more structural difference compared to **1**.

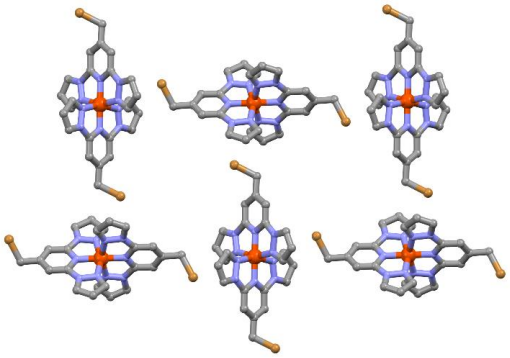

Figure 3. Crystal packing for **1·4MeNO₂**.

The presence of nitromethane molecules in the crystal induced drastic change for the stack of the complexes since the π···π and Br···Br contacts are lost (Figure 3). The crystal packing highlighted perpendicular arrangement of the complexes. The section on the magnetic properties will show the consequence of the structural changes between the two complexes.

$[Co(L)_2](BF_4)_2$·2MeNO₂ (2·2MeNO₂).

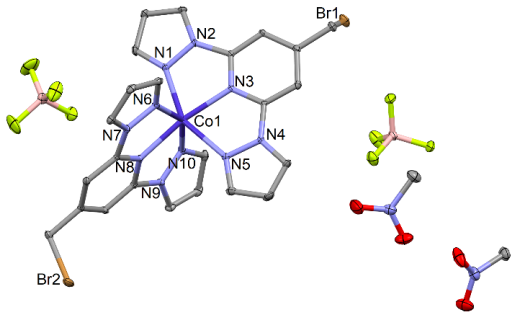

Figure 4. Ortep View of the structure of **Co·2MeNO₂**. Atomic displacement ellipsoids are drawn at the 30% probability level. Hydrogen atoms are omitted for clarity.

Co·2MeNO₂ crystallizes in the triclinic space group P-1 (N°2) (Table 1). The ORTEP view of **Co·2MeNO₂** is shown in Figure 4. The asymmetric unit is composed of one molecule of $[Co(\mathbf{L})_2]2+$, two BF_4^- anion and two nitromethane molecules of crystallization. The characteristic compressed octahedral polyhedron is observed with Co-$N_{(py)}$ = 2.066 Å and Co-$N_{(pz)}$ = 2.143(3) Å. Such Co-N bond lengths designated a HS state Co^{II} centre. The longer Co-N distances compared to the Fe-N distances lead to smaller $N_{(pz)}$-Co-$N_{(pz)}$ (149.5(1)° and 150.8(1)°) and $N_{(py)}$-Co-$N_{(py)}$ (170.2(1)°) angles compared to its Fe^{II} analogue. The two L ligands are close to be perpendicular with an angle of 83.0(1)°. Nevertheless while one L is planar (as observed for the two Fe^{II} solvatomorphs) the second one is not. In fact the two plans formed by the pyridine ring and one of the pyrazole unit display an angle of 16.0(1)°.

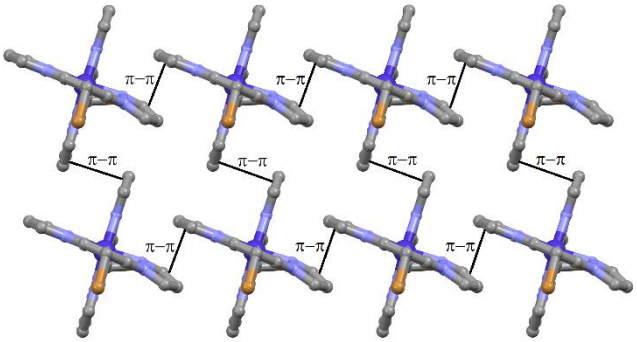

Figure 5. Crystal packing for **2·2MeNO₂**.

The Figure 5 highlighted a regular “terpyridine embrace” crystal packing for **2·2MeNO₂** with CH_2Br groups localized at 68.8° and 81.4° of the plane formed by the bpp fragments.

Magnetic measurements

$[Fe(L)_2](BF_4)_2$ (1). Magnetic susceptibility measurements of **1** shows an abrupt HS (S = 2, $\chi_M T$ = 3.95 cm^3 K mol^{-1}) to LS (S = 0) transition centred around 324 K with a straight thermal hysteresis (4 K). On cooling, the transition occurs at T_C = 326 K while increasing the temperature the transition occurs at 322 K. Such abrupt transition with a straight magnetic bistability are associated with the ”terpyridine embrace” crystal packing form and an octahedral coordination sphere characterized by the two angles ϕ = 180° and θ = 90°[9] in the HS state of **1** complex. The spin transition temperature is higher than the room temperature which is surprising since the analogue complex with two hydrogen atoms instead of the bromide atoms highlighted a spin transition centred at 207 K.[9] Such substitution and the resulting Br···Br short contacts clearly stabilize the LS state of **1**.

$[Fe(L)_2](BF_4)_2$·4MeNO₂ (1·4MeNO₂). The magnetic properties of the solvated derivative showed a more progressive spin transition around 340 K with a wider thermal hysteresis (35 K) compared to the unsolvated derivative (Figure 6). Based on the previous

Halcrow's works, the difference of hysteresis width and temperature of transition could be attributed to both solvation[8] and a moderate Jahn-Teller distortion of the HS state[10] for **1·4MeNO₂**. Unfortunately the complete thermal spin crossover is localized at to high temperature (T > 400 K) to perform data collection and refinement of the HS state structure for **1·4MeNO₂**. It is worth to notice that the **1·4MeNO₂** compound presents the widest hysteresis loop measured for a $[Fe(bpp\text{-}R)_2]^{2+}$ derivatives since the previous record was measured at 18 K for the methyl-substituted analogue.[9] The form of the crystal packing imposed by the orientation of the bromide substitutions and the presence of nitromethane molecules of crystallization might be the origin of a such large hysteresis loop. In addition, one can observe that the $\chi_M T$ product decreased in cooling mode in a six-step manner centred at 265, 280, 295, 315, 335 and 355 K (see the derivative of the data plot in Figure S1). The hysteresis loop remains open after several warming cycle and it cannot be attributed to desolvation or irreversible crystallographic phase transition (Figure S2). Such multiple spin-state conversions was already observed in warming mode for the $[Fe(bpp)_2][Ni(mnt)_2]_2{\cdot}MeNO_2$ compound (where mnt = maleonitriledithiolate)[27] and in both cooling and warming modes for the $[Fe(bppMe)_2](BF_4)_2{\cdot}xH_2O$ (bppMe = 2,6-bis(3-methylpyrazol-1-yl)pyridine)[28].

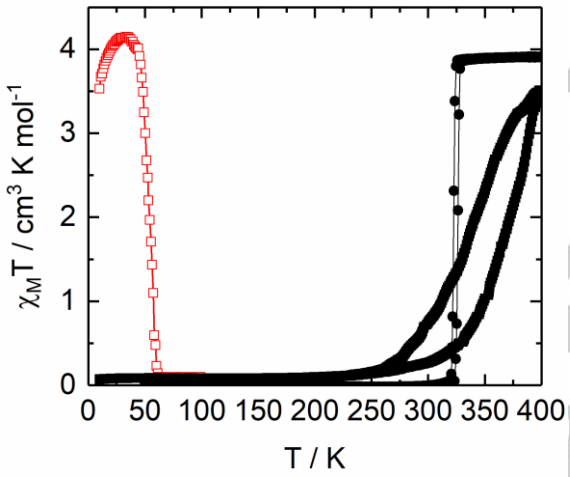

Figure 6. Thermal dependence of $\chi_M T$ for **1** (full circles), **1·4MeNO₂** (full square). The thermal dependence of $\chi_M T$ **1·4MeNO₂** after light irradiation (660 nm, 5 mW) is represented with red squares.

The red data plots of the Figure 6 shows the results of the irradiation at 660 nm in the tail of the absorption band which corresponds to the *d-d* and/or Metal-to-Ligand Charge Transfer (MLCT) transitions of the LS state of **1·4MeNO₂** (Figure S3). After 5 min of light irradiation at 10 K, almost all the LS fraction is converted in HS by population of the metastable $^5T_{2g}$ (Oh) state. Switching off the light leads to a population of the metastable $^5T_{2g}$ which persists up to T_{LIESST} = 55 K at a sweep rate of 0.3 K min^{-1}. This value is lower than the T_{LIESST} measured under a light irradiation of 510 nm for the two solvatomorphs of the methyl-substituted-bpp analogues (87 and 112 K).[9] This experimental observation is perfectly in agreement with the linear relation ($T_{LIESST} = T_0\text{-}0.3T_{1/2}$)[28] which connects photomagnetism and thermal spin crossover and saying that higher the $T_{1/2}$ is found lower the T_{LIESST} will be determined. $T_{1/2}$ is the thermal spin transition temperature, T_{LIESST} is the light-induced excited spin state trapping temperature and T_0 is an empirical parameter determined equal to 150 K for meridional tridentate ligands[29]. Using such relation, a $T_{1/2}$ = 340 K should lead to a T_{LIESST} = 48 K which is a value close to the experimental T_{LIESST} = 55 K.

$[Co(L)_2](BF_4)_2{\cdot}2MeNO_2$ (2·2MeNO₂). The magnetic properties of **2·2MeNO₂** were probed measuring the magnetic susceptibility for an immobilized crystalline powder of the sample. The temperature dependence of the $\chi_M T$ product is depicted in the Figure S3. The room temperature value of 3.19 cm^3 K mol^{-1} is larger than the expected spin-only value (1.875 cm^3 K mol^{-1}) for high-spin Co^{II} ion. Nevertheless this experimental value is in agreement with the value range of 2.1-3.4 cm^3 K mol^{-1} for an highly anisotropic Co^{II} ions including a strong orbital angular momentum contribution.[29] Upon cooling, the $\chi_M T(T)$ curve decreases monotonously to reach a value of 2.30 cm^3 K mol^{-1} at 2 K. The decreasing is mainly due to the magnetic anisotropy of the Co^{II} with possible additional antiferromagnetic intermolecular interactions at low temperature.

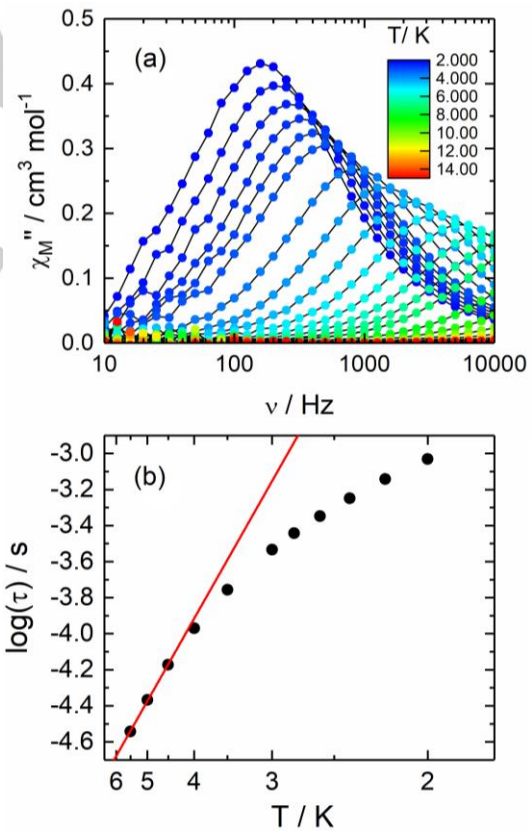

Figure 7. (a) Frequency dependence of the out-of-phase component of the magnetic susceptibility for **2·2MeNO₂** between 2 and 14 K under an applied DC field of 1000 Oe. (b) Arrhenius plot of the thermal dependence of the relaxation time of the magnetization. The red line represents a fit for the high-temperature region.

The magnetic field dependence of the magnetization at 2 K between 0 and 50 kOe is depicted in inset of the Figure S4. At the maximum field value the magnetization takes the value of 2.50 μ_B but without reaching a saturation sign of significant magnetic anisotropy. Consequently the magnetic relaxation dynamics were probed by measuring the frequency-dependence ac susceptibility below 15 K. No out-of-phase component of the magnetic susceptibility was detected under zero dc field. Nevertheless application of a moderated dc field provokes the appearance of an out-of-phase which is centred at 160 Hz at 2 K for the optimal dc field of 1000 Oe (Figure S5). Such cancelling of the tunnelling magnetic relaxation is very common for Co^{II}-based SMM. The compound **2·2MeNO₂** displayed typical field-induced mononuclear SMM under an applied dc field of 1000 Oe (Figures S6 and 7a). From the frequency dependence of the magnetic susceptibility is generated the Cole-Cole plots below 14 K (Figure S7). The values (α) and the distribution of relaxation time (τ) were extracted using a generalized Debye model (Table S1)[31] while the energy barrier Δ was evaluated from the linear fit of the high temperature region of the Arrhenius plot (Orbach regime) (Figure 8b). Using the following equation $\tau = \tau_0 \exp(U_{eff}/k_BT)$, the best fit gives U_{eff} = 14.6(4) cm^{-1} and $\tau_0 = 6.28(8) \times 10^{-7}$ s. The α values range from 0.02 to 0.12 suggesting a narrow distribution of the relaxation time.

Conclusions

The association of the ligand 2,6-di(pyrazol-1-yl)-4-(bromomethyl)pyridine (**L**) with the divalent metallic ion Fe(II) and Co(II) led to the formation of mononuclear complexes of formula $[M(\mathbf{L})_2](BF_4)_2 \cdot x MeNO_2$. The Fe^{II} based compound crystallized in two solvatomorphs $[Fe(\mathbf{L})_2](BF_4)_2$ (**1**) and $[Fe(\mathbf{L})_2](BF_4)_2 \cdot 4MeNO_2$ (**1·4MeNO₂**). The LS Fe^{II} crystal structure of the unsolvated derivative highlighted a partial "terpyridine embrace" type crystal packing while the solvated derivative did not. As a consequence, both solvatomorphs displayed thermal Spin Crossover at high temperature ($T_{1/2}$ = 320-340 K) nevertheless the one for **1** presented an abrupt spin transition with a straight hysteresis loop while **1·4MeNO₂** presented a more gradual spin transition with the widest thermal hysteresis (35 K) for this type of complexes. In addition the spin transition in cooling mode operated in a six-step manner. Finally the **1·4MeNO₂** solvatomorph is photo-active with an efficient LIESST effect under light irradiation at 530 nm and T_{LIESST} = 55 K. The $[Co(\mathbf{L})_2](BF_4)_2 \cdot 2MeNO_2$ (**1·2MeNO₂**) complex did not show any spin transition but the dynamic magnetic properties highlighted a mononuclear SMM behaviour under an applied dc field of 1000 Oe with an effective energy barrier of 14.6(4) cm^{-1} and a relaxation time of $6.28(8) \times 10^{-7}$ s. Both Fe^{II} and Co^{II} derivatives shown promising magnetic properties and they could be used as metallo-precursors for further functionalization thank the bromo-methyl groups.

Experimental Section

Synthesis. General Procedures and Materials. The ligand 2.6-di(pyrazol-1-yl)-4-bromomethyl)pyridine (**L**)[14] was synthesized following previously reported methods. All other reagents were purchased from Acros, Alfa Aesar, Aldrich Co., Ltd. and used without further purification.

Synthesis of $[Fe(L)_2](BF_4)_2 \cdot x MeNO_2$ (x = 0 (1) and x = 4 (1·4MeNO₂). 50.6 mg of $Fe(BF_4)_2 \cdot 6H_2O$ (0.15 mmol) and 91.2 mg of L (0.30 mmol) were dissolved in 15 mL of CH_3NO_2 and heated to reflux for 3 h under argon atmosphere. After cooling to room temperature, the solution was stirred overnight and then concentrated to a volume of c.a. 7.5 mL. The resulting brown solution was divided in 5 glass hemolysis tubes and slow diffusion of Et_2O vapour led to the formation of brown plate (x=0) and prism (x=4) single crystals suitable for X-ray analysis. Yield: 73 mg (about 54 % based on single crystals). Anal. Calcd (%) for C24H20F8FeN10Br2B2: C 34.36, H 2.39, N 16.71; found: C 34.39, H 2.44 N, 16.54. Anal. Calcd (%) for C28H32F8FeN14O8Br2B2 C 31.05, H 2.96, N 18.11; found: C 31.09, H 3.07 N, 18.04. I.R. (KBr): 3128 (w), 3093 (w), 3022 (w), 2965 (w), 2918 (w), 1620 (s), 1577 (s), 1522 (m), 1467 (s), 1399 (s), 1262 (m), 1207 (m), 1114 (w), 1084 (m), 1042 (s), 958 (m), 918 (w), 860 (w), 789 (m), 764 (s), 672 (w), 643 (w), 606 (w) and 566 (w) cm^{-1}.

Synthesis of $[Co(L)_2](BF_4)_2 \cdot 2MeNO_2$ (2·2MeNO₂). Similar experimental procedure than for the Fe^{II} derivatives was used except that 51.3 mg of $Co(BF_4) \cdot 6H_2O$ was employed instead of $Fe(BF_4)_2 \cdot 6H_2O$. The resulting yellow-brownish solution was divided in 5 glass hemolysis tubes and slow diffusion of Et_2O vapour led to the formation of yellow board single crystals suitable for X-ray analysis. Yield: 85 mg (about 59 % based on single crystals). Anal. Calcd (%) for C26H26F8CoN12O4Br2B2: C 34.42, H 1.68, N 4.15; found: C 34.69, H 1.74 N, 4.14. I.R. (KBr): 3130 (w), 3089 (w), 3063 (w), 3039 (w), 3009 (w), 2915 (w), 1638 (s), 1580 (s), 1525 (m), 1471 (s), 1404 (s), 1339 (m), 1310 (m), 1285 (m), 1174 (m), 1114 (w), 1084 (m), 1042 (s), 969 (m), 915 (w), 860 (w), 770 (m), 678 (w), 641 (w), 598 (m), 524 (w) and 448 (w) cm^{-1}.

X-ray diffraction. Single crystal of **1**, **1·4MeNO₂** and **2·2MeNO₂** were mounted on a APEXIII D8 VENTURE Bruker-AXS diffractometer for data collection (MoKα radiation source, λ = 0.71073 Å), from the Centre de Diffractométrie (CDIFX), Université de Rennes 1, France (Table 1). Structure was solved with a direct method using the SHELXT program[32] and refined with a full matrix least-squares method on F2 using the SHELXL-14/7 program[33]. Complete crystal structure results as a CIF file including bond lengths, angles, and atomic coordinates are deposited as Supporting Information.

Physical Measurements. The elementary analyses of the compounds were performed at the Centre Régional de Mesures Physiques de l'Ouest, Rennes. Single crystals of **1**, **1·4MeNO₂** and **2·2MeNO₂** are manually selected and their cell parameters are checked before magnetic measurements. The dc magnetic susceptibility measurements were performed on grinded previously selected single crystal in Teflon tape with a Quantum Design MPMS-XL SQUID magnetometer between 2 and 300 K in applied magnetic field of 0.02 T in the temperature range 2-20 K, 0.2 T in the temperature range 20-80 K and 1 T above 80 K. These measurements were all corrected for the diamagnetic contribution of the Teflon tape and the intrinsic diamagnetism calculated with Pascal's constants.

Acknowledgements

We acknowledge financial support from CNRS, Université de Rennes 1 and ERC Consolidator Grant MULTIPROSMM (Proj. no. 725184).

Keywords: Iron • Cobalt • dipyrazolylpyridine • Single-Molecule Magnet • Spin Crossover

[1] a) L. Bogani, W. Wernsdorfer, *Nat. Mater.* **2008**, *7*, 179–186; b) M. N. Leuenberger, D. Loss, *Nature* **2001**, *410*, 789–793; c) J. Lehmann, A. Gaita-Arino, E. Coronado, D. Loss, *J. Mater. Chem.* **2009**, *19*, 1672–1677; d) O. Kahn, C. J. Martinez, *Science* **1998**, *279*, 44–48.

[2] a) R. Sessoli, D. Gatteschi, A. Caneschi, M. A. Novak, *Nature* **1993**, *365*, 141–143; b) G. Aromi, E. K. Brechin, in Single-Molecule Magnets and Related Phenomena, ed. R. Winpenny, 2006, p. 1–67.

[3] a) P. Gütlich, Y. Garcia, H. A. Goodwin, *Chem. Soc. Rev.* **2000**, *29*, 419–427; b) A. Bousseksou, G. Molnar, L. Salmon, W. Nicolazzi, *Chem. Soc. Rev.* **2011**, *40*, 3313–3335; c) M. C. Munoz, J. A. Real, *Coord. Chem. Rev.* **2011**, *255*, 2068–2093; d) G. Aromí, L. A. Barrios, O. Roubeau, P. Gamez, *Coord. Chem. Rev.* **2011**, *255*, 485–546; e) M. A. Halcrow, *Chem. Soc. Rev.* **2011**, *40*, 4119–4142; f) M. A. Halcrow *Spin-Crossover Materials-Properties and Applications*, ed. John Wiley & Sons, Ltd.: New York, **2013**.

[4] L. Cambi, A. Gagnasso, *Atti. Accad. Naz. Lincei* **1931**, *13*, 809-813.

[5] a) S. Decurtins, P. Gütlich, C. P. Köhler, H. Spiering, A. Hauser, *Chem. Phys. Lett.* **1984**, *105*, 1–4; b) P. Gütlich, A. Hauser, H. Spiering, *Angew. Chem., Int. Ed.* **1994**, *33*, 2024–2054; c) J.-F. Létard, *J. Mater. Chem.* **2006**, *16*, 2550–2559.

[6] a) Spin Crossover in Transition Metal Compounds I−III, Topics in Current Chemistry; Gütlich, P., Goodwin, H. A., Eds.; Springer-Verlag: Berlin, **2004**; Vols. 233−235; b) A. Bousseksou, G. Molnár, L. Salmon, W. Nicolazzi, *Chem. Soc. Rev.* **2011**, *40*, 3313−3335; c) M. Cavallini, *Phys. Chem. Chem. Phys.* **2012**, *14*, 11867−11876; d) H. J. Shepherd, G. Molnar, W. Nicolazzi, L. Salmon, A. Bousseksou, *Eur. J. Inorg. Chem.* **2013**, 653−661; e) M. C. Munoz, J. A. Real, *Coord. Chem. Rev.* **2011**, *255*, 2068−2093. f) J. Tao, R.-J. Wei, R.-B. Huang, L.-S. Zheng, *Chem. Soc. Rev.* **2012**, *41*, 703−737; g) Gütlich, P. Eur. J. Inorg. Chem. 2013, 581−591. h) P. Gütlich, A. B. Gaspar, Y. Garcia, *Beilstein J. Org. Chem.* **2013**, *9*, 342−391.

[7] L. J. Kershaw Cook, R. Kulmaczewski, S. A. Barrett, M. A. Halcrow, *Inorg. Chem. Front.* **2015**, *2*, 662-670.

[8] a) L. J. Kershaw Cook, R. Kulmaczewski, O. Cespedes, M. A. Halcrow, *Chem. Eur. J.* **2016**, *22*, 1789-1799; b) M. Fumanal, F. Jiménez-Gravalos, J. Ribas-Arino, S. Vela, *Inorg. Chem.* **2017**, *56*, 4474-4483.

[9] L. J. Kershaw Cook, F. L. Thorp-Greenwood, T. P. Comyn, O. Cespedes, G. Chastanet, M. A. Halcrow, *Inorg. Chem.* **2015**, *54*, 6319-6330.

[10] L. J. Kershaw Cook, R. Mohammed, G. Sherborne, T. D. Roberts, S. Alvarez, M. A. Halcrow, *Coord. Chem. Rev.* **2015**, *289-290*, 2-12.

[11] N. Ishikawa, M. Sugita, T. Ishikawa, S. Koshihara, Y. Kaizu, *J. Am. Chem. Soc.* **2003**, *125*, 8694-8695.

[12] R. Ishikawa, R. Miyamoto, H. Nojiri, B. K. Breedlove, M. Yamashita, *Inorg. Chem.* **2013**, *52*, 8300-8302 ; b) A. Grigoropoulous, M. Pissas, P. Rapatolis, V. Psycharis, P. Kyritsis, Y. Sanakis, *Inorg. Chem.* **2013**, *52*, 12869-12871 ; c) J. Vallejo, A. Pascual-Alvarez, J. Cano, I. Castro, M. Julve, F. Lloret, J. Krzystek, G. De Munno, D. Armentano, W. Wernsdorfer, R. Ruiz-Garcia, E. Pardo, *Angew. Chem., Int. Ed.* **2013**, *52*, 14075-14079.

[13] S. Mossin, B. L. Tran, D. Adhikari, M. Pink, F. W. Heinemann, J. Sutter, R. K. Szilagyi, K. Meyer, D. J. Mindiola, *J. Am. Chem. Soc.* **2012**, *134*, 13651-13661.

[14] a) W. H. Harman, T. D. Harris, D. E. Freedman, H. Fong, A. Chang, J. D. Rinehart, A. Ozarowski, M. T. Sougrati, F. Grandjean, G. J. Long, J. R. Long, *J. Am. Chem. Soc.* **2010**, *132*, 18115-18126; b) D. E. Freedman, W. H. Harman, T. D. Harris, G. J. Long, C. J. Chang, J. R. Long, *J. Am. Chem. Soc.* **2010**, *132*, 1224-1225; c) D. Weismann, Y. Sun, Y. Lan, G. Wolmershauser, A. K. Powell, H. Sitzmann, *Chem. Eur. J.* **2011**, *17*, 4700-4704; d) P.-H. Lin, N. C. Smythe, S. J. Gorelsky, S. Maguire, N. J. Henson, I. Korobkov, B. L. Scott, J. C. Gordon, R. T. Baker, M. Murugesu, *J. Am. Chem. Soc.* **2011**, *133*, 15806-15809.

[15] J. M. Zadrozny, D. J. Xiao, M. Atanasov, G. J. Long, F. Grandjean, F. Neese, J. R. Long, *Nat. Chem.* **2013**, *5*, 577-581.

[16] R. C. Poulten, M. J. Page, A. G. Algarra, J. J. Le Roy, I. Lopez, E. Carter, A. Llobet, S. A. Macgregor, M. F. Mahon, D. M. Murphy, M. Murugesu, M. K. Whittlesey, *J. Am. Chem. Soc.* **2013**, *135*, 13640-13643.

[17] J. Miklovič, D. Valigura, R. Boča, J. Titiš, *Dalton Trans.* **2015**, *44*, 12484-12487.

[18] Y.-S. Meng, Z. Mo, B.-W. Wang, Y.-Q., L. Deng, S. Gao, *Chem. Sci.* **2015**, *6*, 7156-7162.

[18] a) A. Eichhofer, Y. Lan, V. Mereacre, T. Bodenstein, F. Weigend, *Inorg. Chem.* **2014**, *53*, 1962-1974; b) J. M. Zadrozny, J. R. Long, *J. Am. Chem. Soc.* **2011**, *133*, 20732-20734; c) J. M. Zadrozny, J. Liu, N. A. Piro, C. J. Chang, S. Hill, J. R. Long, *Chem. Commun.* **2012**, *48*, 3927-3929; d) F. Yang, Q. Zhou, Y. Zhang, G. Zeng, G. Li, Z. Shi, B. Wang, S. Feng, *Chem. Commun*. **2013**, *49*, 5289-5291; e) R. Boča, J. Miklovič, J. Titiš, *Inorg. Chem.* **2014**, *53*, 2367-2369; f) T. Jurca, A. Farghal, P.-H. Lin, I. Korobkov, M. Murugesu, D. S. Richeson, *J. Am. Chem. Soc.* **2011**, *133*, 15814-15817; g) F. Habib, O. R. Luca, V. Vieru, M. Shiddiq, I. Korobkov, S. I. Gorelsky, M. K. Takase, L. F. Chibotaru, S. Hill, R. H. Crabtree, M. Murugesu, *Angew. Chem., Int. Ed.* **2013**, *52*, 11290-11293; h) J. Vallejo, I. Castro, J. Ruiz-Garcia, J. Cano, M. Julve, F. Lloret, G. De Munno, W. Wernsdorfer, E. Pardo, *J. Am. Chem. Soc.* **2012**, *134*, 15704-15707; i) E. Colacio, K. Ruiz, E. Ruiz, E. Cremades, J. Krzystek, S. Carretta, J. Cano, T. Guidi, W. Wernsdorfer, E. K. Brechin, *Angew. Chem., Int. Ed.* **2013**, *52*, 9130-9134; j) Y.-Y. Zhu, C. Cui, Y.-Q. Zhang, J.-H. Jia, X. Guo, C. Gao, K. Qian, S.-D. Jiang, B.-W. Wang, Z.-M. Wang, S. Gao, *Chem. Sci.* **2013**, *4*, 1802-1806; k) I. A. Gass, S. Tewary, A. Nafady, N. F. Chilton, C. J. Gartshore, M. Asadi, D. W. Lupton, B. Moubaraki, A. M. Bond, J. F. Boas, S.-X. Guo, G. Rajaraman, K. S. Murray, *Inorg. Chem.* **2013**, *52*, 7557-7572; l) R. Herchel, L. Váhovská, I. Potočňák, Z. Trávníček, *Inorg. Chem.* **2014**, *53*, 5896-5898; m) T. J. Woods, M. F. Ballesteros-Rivas, S. Gomez-Coca, E. Ruiz, K. R. Dunbar, *J. Am. Chem. Soc.* **2016**, *138*, 16407-16416.

[20] L. Chen, J. Wang, J.-M. Wei, W. Wernsdorfer, S.-T. Chen, Y.-Q. Zhang, Y. Song, Z.-L. Xue, *J. Am. Chem. Soc.* **2014**, *136*, 12213-11216.

[21] X.-N. Yao, J.-Z. Du, Y.-Q. Zhang, X.-B. Leng, M.-W. Yang, S.-D. Jiang, Z.-X. Wang, Z.-W. Ouyang, L. Deng, B.-W. Wang, S. Gao, *J. Am. Chem. Soc.* **2017**, *139*, 373-380.

[22] C. Rajnak, J. Titiš, O. Fuhr, M. Ruben, R. Boča, Inorg. Chem. 2014, 53, 8200-8202.

[23] T. Ayers, S. Scott, J. Goins, N. Caylor, D. Hathcock, S. J. Slattery, D. L. Jameson, *Inorg. Chimica Acta* **2000**, *307*, 7-12.

[24] a) M. Feng, F. Pointillart, B. Lefeuvre, V. Dorcet, S. Golhen, O. Cador, L. Ouahab, *Inorg. Chem.* **2015**, *54*, 4021-4028; b) S. Speed, M. Feng, G. Fernandez Garcia, F. Pointillart, B. Lefeuvre, F. Riobé, S. Golhen, B. Le Guennic, F. Totti, Y. Guyot, O. Cador, O. Maury, L. Ouahab, *Inorg. Chem. Front.* **2017**, *4*, 604-617.

[25] a) M. L. Scudder, H. A. Goodwin, I. G. Dance, *New J. Chem.* **1999**, *23*, 695-705; b) R. Pritchard, C. A. Kilner, M. A. Halcrow, *Chem. Commun.* **2007**, 577-579; c) I. Dance, M. Scudder, *CrystEngComm* **2009**, *11*, 2233-2247.

[26] R. Mohammed, G. Chastanet, F. Tuna, T. L. Malkin, S. A. Barret, C. A. Kilner, J.-F. Létard, M. A. Halcrow, *Eur. J. Inorg. Chem.* **2013**, 819-831.

[27] M. Nihei, H. Tahira, N. Takahashi, Y. Otake, Y. Yamamura, K. Saito, H. Oshio, J. Am. Chem. Soc. 2010, 132, 3553-3560.

[28] V. A. Money, C. Carbonera, J. Elhaïk, M. A. Halcrow, J. A. K. Howard, J.-F. Létard, *Chem. Eur. J.* **2007**, *13*, 5503-5514.

[29] a) S. Marcén, L. Lecren, L. Capes, H. A. Goodwin, J.-F. Létard, *Chem. Phys. Lett.* **2002**, *358*, 87-95; b) V.A. Money, J. S. Costa, S. Marcén, G.

10.1002/ejic.201800819

Chastanet, J. Elhafflk, M.A. Halcrow, J. A. K. Howard, J.-F. Létard, *Chem. Phys. Lett*. **2004**, *391*, 273-277; c) C. Carbonera, J. S. Costa, V. A. Money, J. Elhafflk, J. A. K. Howard, M. A. Halcrow, J.-F. Létard, *Dalton Trans.* **2006**, 3058-3066.

[30] F. E. Mabbs, D. J. Machin, *Magnetism and Transition Metal Complexes*; Dover Publications: Mineola, NY, **2008**.

[31] K. S. Cole, R. H. Cole, *J. Chem. Phys.* **1941**, *9*, 341-351.

[32] G. M. Sheldrick, *Acta Crystallogr. Sect. A* **2015**, *71*, 3−8.

[33] G. M. Sheldrick, *Acta Crystallogr. Sect. C* **2015**, *71*, 3-8.

10.1002/ejic.201800819

FULL PAPER

The three mononuclear complexes of Fe^{II} and Co^{II} involving the 2,6-di(pyrazol-1-yl)-4-(bromomethyl)pyridine (**L**) displayed thermal and photo-induced spin transition, and field-induced Single-Molecule Magnet behaviour respectively.

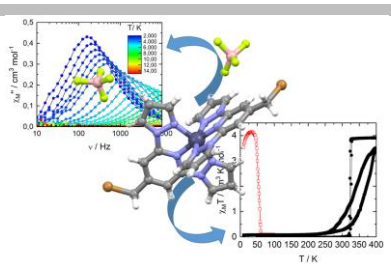

Co^{II} SMM and Fe^{II} Spin CrossOver

Haiet Douib, Louis Cornet, Jessica Flores Gonzalez, Elzbieta Trzop, Vincent Dorcet, Abdelkrim Gouasmia, Lahcène Ouahab, Olivier Cador, Fabrice Pointillart,**

Page No. – Page No.

Spin Crossover and Field-Induced Single-Molecule Magnet Behaviour in Metal(II)-Dipyrazolylpyridine Complexes